Regularization of softening plasticity with the cumulative plastic strain-rate gradient

G. Bacquaert, Jeremy Bleyer, C. Maurini

Regularization of softening plasticity with the cumulative plastic strain-rate gradient

G. Bacquaert[a,*], J. Bleyer[b], C. Maurini[c]

[a] *Électricité de France, R&D Division, Palaiseau, France*
[b] *École Nationale des Ponts et Chaussées, Université Gustave Eiffel, CNRS, Laboratoire Navier, UMR 8205, Marne-la-Vallée, France*
[c] *Sorbonne Université, CNRS, Institut Jean Le Rond d'Alembert, UMR 7190, Paris, France*

Abstract

We propose a novel variational framework to regularize softening plasticity problems. Specifically, we modify the plastic dissipation potential term by adding a contribution depending on the cumulative plastic strain-rate gradient. We formulate the evolution of the so-obtained strain-rate gradient plasticity model with an incremental variational principle. The time-discretized evolution equations are deduced from the corresponding first-order optimality conditions. To investigate the model, the problem of a bar in traction is studied. Analytical solutions are explicitly derived, and characterized by exponential localization profiles. Contrary to other regularization strategies, no spurious spreading of the plastic localization band is observed. A first numerical implementation in 1D and 2D plane strain conditions is proposed based on conic programming solvers and validated against the analytical predictions. Numerical results on plane strain von Mises plasticity show that the proposed framework leads to mesh-independent results and efficient control of plastic localization bands.

Keywords: Softening plasticity; Strain localization; Regularization of constitutive models; Generalised Standard Materials ; Variational principle

1. Introduction

Local constitutive models fall short to be predictive of softening, showing pathological mesh-dependency in finite element computations. In the context of brittle fracture, variational models including the gradient of a damage variable have been shown efficient to limit the occurrence of spurious localization by considering additional penalization terms to the total energy (Bourdin et al., 2000, 2008; Pham et al., 2011), models which have been more recently extended in the context of ductile fracture (Alessi et al., 2015, 2018; Miehe et al., 2016). As softening plasticity is concerned, the influential work of (Aifantis, 1987) paved the way to advance gradient theories, considering non-local models (Pijaudier-Cabot and Bažant, 1987; Engelen et al., 2003), higher-order gradient models (Chambon et al., 1998; Fernandes, 2008; Maugin, 1990; Frémond and Nedjar, 1996; Lorentz and Andrieux, 1999), or models with enriched kinematics (Mühlhaus and Vardoulakis, 1987; Forest, 2009). Comprehensive overviews of these theories can now be found in (Russo et al., 2020; Nguyen, 2021; Besson

*Corresponding author
Email address: goustan.bacquaert@edf.fr (G. Bacquaert)

et al., 2023).

Within the framework of Generalized Standard Materials (Halphen and Nguyen, 1975), the introduction of the gradient of an internal variable has been proposed (Maugin, 1990; Frémond and Nedjar, 1996). It allows to benefit from a variational structure deriving from the corresponding energy and dissipation potentials (Lorentz and Andrieux, 1999; Nguyen, 2021). The most common approach to introduce a gradient effect in plasticity models is to supplement the free energy with a quadratic term of the plastic strain gradient such as (Aifantis, 1987; Gurtin and Anand, 2009):

$$\psi_{\text{reg}}(\boldsymbol{\varepsilon}, \boldsymbol{\varepsilon}^p, p, \nabla p) = \psi_{\text{loc}}(\boldsymbol{\varepsilon}, \boldsymbol{\varepsilon}^p, p) + \frac{A}{2}\|\nabla p\|^2, \quad \text{with} \quad p = \int_0^t \|\dot{\boldsymbol{\varepsilon}}^p\| \mathrm{d}t, \tag{1}$$

where $\psi_{\text{loc}}(\boldsymbol{\varepsilon}, \boldsymbol{\varepsilon}^p, p)$ is the original free energy of the local model. The material parameter $A > 0$ sets a typical length scale to control plastic strain localization. This quadratic plastic gradient regularization can be seen as a limit case of micromorphic models (Forest, 2009). It has been used by many authors to control the plastic localization also because its numerical implementation is relatively simple.

Nevertheless, several works pointed out the inherent drawbacks of the quadratic regularization approach for softening plasticity (Jirásek and Rolshoven, 2009a; Scherer et al., 2019; Abatour and Forest, 2023). The main issue is that the localized plastic bands eventually spread in an uncontrolled manner in the case of non-linear softening when increasing the loading. This is illustrated in Figure 1 for the case of a one-dimensional bar in traction using a bilinear softening model (Jirásek and Rolshoven, 2009b). To mitigate these issues, Forest and co-workers proposed to add an *ad hoc* evolution equation of the internal length scale (Scherer et al., 2019) or to introduce a saturation of the state variables (Abatour and Forest, 2023). In contrast, limited efforts have been made to introduce the gradient of an internal variable rate into the dissipation potential within the context of the regularization of softening. The few attempts include the use of an integral condition on the rate of change of the void volume fraction for porous plasticity (Needleman and Tvergaard, 1998), or the work of (Andrieux et al., 1996) exploring the use of a damage-rate gradient within a variational consistent approach. Surprisingly, models including the gradient of a plastic strain-rate in the dissipation potential are more common in works dealing with size and strengthening effects, leading to higher yield stresses for small-size specimens (Fleck et al., 1994; Anand et al., 2005; Reddy and Sysala, 2023).

The objective of this paper is to investigate a novel approach to softening plasticity, introducing the regularization through the cumulative plastic strain-rate gradient in the dissipation potential. As discussed before, this is in contrast to the majority of approaches considering the plastic strain gradient in the free energy as a localization limiter. Our developments will be based on the framework of Generalized Standard Materials (GSM), thereby benefiting from a consistent variational formulation.

We propose a whole class of models depending on the specific choice of the regularizing term. First, we restrict our attention to a specific choice in a one-dimensional (1D) formulation, which enables to obtain analytical solutions. We discuss the resulting plastic

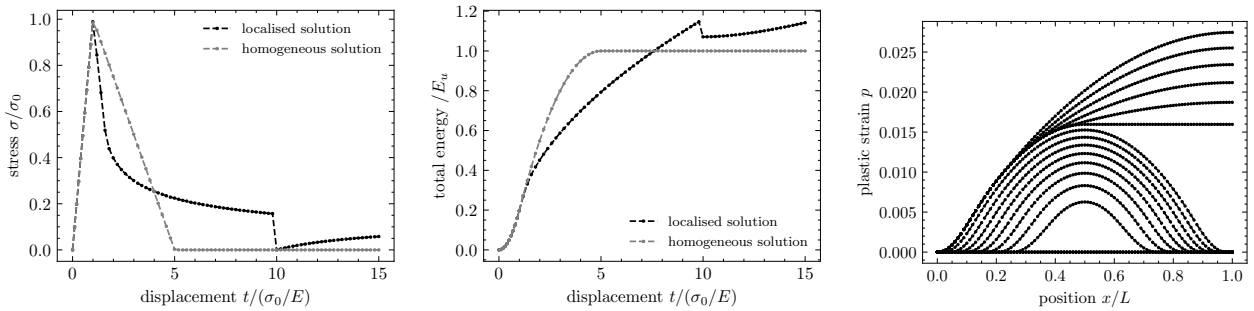

(a) Stress-strain response.

(b) Total energy evolutions.

(c) Plastic strain profiles of the localised solution.

Figure 1: Examples of numerical responses of a bar of length L in traction using a bilinear softening plasticity model, regularized by a quadratic plastic gradient as in eq. (1) (the simulation is carried out by numerical tools briefly described in Section 4). In the legends, σ_0 denotes the initial yield stress, E is the elastic modulus and E_u is the ultimate energy predicted by the homogeneous solution at which the stress is zero. As we observe in Figure 1c, the width of the localisation band, initially symmetric with respect to the middle of the bar of length L, increases until reaching the extremities of the bar. At this instant, symmetry is lost and both the stress and the total energy show an unstable evolution in Figures 1a and 1b. Interestingly, the total energy computed by the localised solution exceeds the total energy of the homogeneous response at some prescribed displacement level. This phenomenon is qualified as a *locking effect* in (Jirásek and Rolshoven, 2009b).

localization profiles, stress responses and energy evolutions. In a second step, we analyze other choices on the 1D traction case using a numerical resolution. Finally, we sketch the relevance of the model in a plane strain two-dimensional (2D) simulation.

The paper is structured as follows. Section 2 introduces the incremental variational formulation of the plasticity model in a simple 1D problem. We first recall the minimization problem and the first-order optimality conditions related to the local constitutive model under investigation. We then discuss the effects of adding a q–norm of the cumulative plastic strain-rate gradient into the dissipation potential. In Section 3, we restrict our attention to the $q = \infty$ case in order to exhibit analytical solutions over a bar in traction, first for any negative isotropic hardening and then in more depth for bilinear softening. Solutions are compared with numerical results in Section 4 and other choices for q are explored. Finally, a 2D application is proposed in Section 5 considering the stretch of a plate in plane strain conditions for von Mises plasticity.

2. Variational formulation of plasticity

This section presents the variational formulation for plasticity including the cumulative plastic strain-rate gradient as a regularizing term in the dissipation potential. As a model problem, we consider a quasi-static evolution of a 1D bar $\Omega = [0, L]$ with imposed displacements $u(0) = 0$, $u(L) = tL$ at the left and right ends. We suppose that the loading parameter t increases monotonically from $t = 0$. The formulation follows the framework of the Generalized Standard Materials (Halphen and Nguyen, 1975; Nguyen, 2011, 2021) for quasi-static rate-independent processes, assuming infinitesimal transformations and isothermal conditions.

As already specified, we focus on the 1D case but, to keep the notation general, we will adopt multidimensional notations for the space derivatives. For example, we denote by u and $\varepsilon = \nabla u$ the scalar displacement and strain fields, where $\nabla(\cdot) = d(\cdot)/dx$ stands for the derivative with respect to the space variable. As usual, we decompose the strain in the sum of the elastic, ε^e, and plastic, ε^p, contributions, $\varepsilon = \varepsilon^e + \varepsilon^p$. The field will depend on a loading parameter t, that will consider as a time-variable, denoting $\dot{(\cdot)} = d(\cdot)/dt$.

2.1. Incremental variational formulation for the local plasticity model

The constitutive behaviour of the local plasticity model, ignoring for now the regularizing gradient term, is determined by a local free energy potential $\psi(\varepsilon, \varepsilon^p, p)$ and a dissipation potential $\phi(\dot{\varepsilon}^p, \dot{p})$:

$$\begin{cases} \psi(\varepsilon, \varepsilon^p, p) = \dfrac{E}{2}(\varepsilon - \varepsilon^p)^2 + V(p) & \text{(2a)} \\ \phi(\dot{\varepsilon}^p, \dot{p}) \quad = \sigma_0 \dot{p} + I_{\mathbb{R}^+}(\dot{p} - |\dot{\varepsilon}^p|), & \text{(2b)} \end{cases}$$

where $V(p)$ is an isotropic hardening function and $\dot{p}$ denotes the cumulative plastic strain-rate, E and σ_0 being the elastic modulus and the initial yield stress, and $I_{\mathbb{R}^+}$ the characteristic function of $\mathbb{R}^+$.

Given the state of the material $(u_n, \varepsilon^p_n, p_n)$ at time t_n and introducing a backward-Euler approximation for the internal variables, the solution $(u_{n+1}, \varepsilon^p_{n+1} = \varepsilon^p_n + \Delta\varepsilon^p, p_{n+1} = p_n + \Delta p)$ at the time step t_{n+1} is defined as the solution of the following time-discretized variational problem (Mialon, 1986; Ortiz and Stainier, 1999):

$$\begin{aligned} \inf_{u, \Delta\varepsilon^p, \Delta p} & \int_0^L \Big[\frac{E}{2}(\nabla u - \varepsilon^p_n - \Delta\varepsilon^p)^2 + V(p_n + \Delta p) + \sigma_0 \Delta p\Big] \mathrm{d}x \\ \text{s.t. } & |\Delta\varepsilon^p| \leq \Delta p \\ & u(0) = 0,\ u(L) = tL. \end{aligned} \tag{3}$$

The first-order optimality conditions for the problem above result in the following set of equations that $(u_{n+1}, \Delta\varepsilon^p, \Delta p)$ must satisfy:

- equilibrium conditions for the stress:

$$\operatorname{div}\sigma = 0, \quad \text{with} \quad \sigma = E(\nabla u_{n+1} - \varepsilon^p_n - \Delta\varepsilon^p), \tag{4}$$

- plasticity yield criterion:

$$|\sigma| \leq \sigma_0 - R, \quad \text{with} \quad R = -V'(p_n + \Delta p), \tag{5}$$

- plastic flow rule:

$$\Delta\varepsilon^p = \Delta p \frac{\sigma}{\sigma_0 - R}, \quad \text{with} \quad \Delta p \geq 0, \tag{6}$$

- plastic consistency condition:

$$(|\sigma| - \sigma_0 + R)\,\Delta p = 0. \tag{7}$$

The plasticity model is *stress-hardening* if the yield stress $\sigma_p = \sigma_0 - R$ in the plasticity yield criterion (5) is an increasing function of the cumulative plastic strain, *i.e.* if the function $V(p)$ is convex. In this case, the energy functional is strictly convex, the solution of the minimization problem (3) exists and is unique, and the displacement field smooth in space. Perfect plasticity is retrieved when $R = V'(p) = 0$. This is the limit case where the plastic strain can be a measure and the displacement can jump on the set where the plastic strain localises (Suquet, 1981). The mathematical problem is well-posed (although its solution is not unique in general). The energy of the localised solution stays finite and non zero, and the solution can be approximated by standard finite-element techniques. Vice-versa, if $V(p)$ is a concave function, the model is *stress-softening* (negative isotropic hardening). In this case, the minimization problem (3) is ill-posed (it does not admit solutions) and needs some form of regularization (see e.g. de Borst et al., 1993)

2.2. Incremental variational formulation of the plasticity with a gradient-dependent dissipation potential

In this work, we treat the case of *stress-softening* plasticity ($V''(p) < 0$) by introducing a regularizing term $\dot{P} = \ell_0 \nabla \dot{p}$ in the dissipation potential depending on the cumulative plastic strain-rate gradient, where ℓ_0 is a constant length-like parameter. We consider the following gradient-dependent dissipation potential, which replaces $\phi(\dot{\varepsilon}^p, \dot{p})$ (2b),

$$\phi(\dot{\varepsilon}^p, \dot{p}, \dot{P}) = \sigma_0 \|(\dot{p}, \dot{P})\|_q + I_{\mathbb{R}^+}(\dot{p} - |\dot{\varepsilon}^p|), \tag{8}$$

where $\|(x, y)\|_q = (|x|^q + |y|^q)^{1/q}$ can be any q–norm with $q \in [1, \infty]$[1].

First, let us highlight that in the case of a homogeneous plastic strain evolution, $\dot{P} = 0$, and $\phi(\dot{\varepsilon}^p, \dot{p}, 0)$ reduces to expression (2b). As a result, the homogeneous solution of the local model is not changed, irrespective of ℓ_0 and the q–norm. Second, the chosen potential remains a convex function of $\dot{p}$ and of its gradient. It is also positively one-homogeneous so that the resulting behavior remains rate-independent. Finally, we propose some modeling flexibility in the choice of q which we will assess later. Note that upon choosing $q = 1$, the proposed gradient-dependent dissipation potential becomes separable in $\dot{p}$ and its gradient, *i.e.* $\sigma_0 \|(\dot{p}, \dot{P})\|_1 = \sigma_0(\dot{p} + |\dot{P}|)$, resulting in a gradient term akin to the Total Variation (TV)

[1]The case $q = \infty$ corresponds to the max norm $\|(x, y)\|_\infty = \max\{|x|, |y|\}$.

of the cumulative plastic strain-rate gradient.

Using eq. (8) as the dissipation potential, the incremental formulation (3) now becomes

$$\begin{aligned} \inf_{u,\Delta\varepsilon^p,\Delta p} & \int_0^L \Big[\frac{E}{2}(\nabla u - \varepsilon_n^p - \Delta\varepsilon^p)^2 + V(p_n + \Delta p) + \sigma_0 \|(\Delta p, \ell_0 \nabla \Delta p)\|_q\Big] \mathrm{d}x \\ \text{s.t. } & |\Delta\varepsilon^p| \leq \Delta p \\ & u(0) = 0,\ u(L) = tL. \end{aligned} \tag{9}$$

Note that since we have now introduced a gradient term of the cumulative plastic strain increment, it is thus possible to impose boundary conditions on Δp on the boundaries $x = 0$ and $x = L$, e.g. Dirichlet boundary conditions $\Delta p = 0$. In the following, we rather choose free boundary conditions on Δp which will translate into Neumann-like boundary conditions on the dual variable associated with the cumulative plastic strain gradient, as discussed later.

Optimality with respect to the displacement yields first the equilibrium condition as in (4). The constrained minimization on the plastic strain variables can then be rewritten as the following min-max problem

$$\begin{aligned} \inf_{\Delta\varepsilon^p,\Delta p,\Delta P} \sup_{Y_{\varepsilon^p},Y_p,Z} & \int_0^L \Big[\frac{E}{2}(\nabla u_{n+1} - \varepsilon_n^p - \Delta\varepsilon^p)^2 + V(p_n + \Delta p) + \sigma_0 \|(\Delta p, \Delta P)\|_q\Big] \mathrm{d}x \\ & - \int_0^L \Big[Y_p \Delta p + Y_{\varepsilon^p} \Delta\varepsilon^p + Z(\Delta P - \ell_0 \nabla \Delta p)\Big] \mathrm{d}x \\ \text{s.t. } & |Y_{\varepsilon^p}| \leq Y_p, \end{aligned} \tag{10}$$

where Y_{ε^p}, Y_p and Z are Lagrange multiplier fields introduced to enforcing the two constraints $|\Delta\varepsilon^p| \leq \Delta p$ and $\Delta P = \ell_0 \nabla \Delta p$. For smooth solutions, we can use the divergence theorem to reformulate the last term $Z\ell_0 \nabla \Delta p$. We obtain

$$\begin{aligned} \inf_{\Delta\varepsilon^p,\Delta p,\Delta P} \sup_{Y_{\varepsilon^p},Y_p,Z} & \int_0^L \Big[\frac{E}{2}(\nabla u_{n+1} - \varepsilon_n^p - \Delta\varepsilon^p)^2 + V(p_n + \Delta p) + \sigma_0 \|(\Delta p, \Delta P)\|_q\Big] \mathrm{d}x \\ & - \int_0^L \Big[Y_p \Delta p + Y_{\varepsilon^p} \Delta\varepsilon^p + Z\Delta P + \ell_0(\operatorname{div} Z)\Delta p)\Big] \mathrm{d}x \\ & + \ell_0 \Big[Z(L)\Delta p(L) - Z(0)\Delta p(0)\Big] \\ \text{s.t. } & |Y_{\varepsilon^p}| \leq Y_p. \end{aligned} \tag{11}$$

We deduce here-under the following first-order optimality conditions by the classical arguments of *Calculus of Variations* (see (Pham et al., 2011) for instance for more applications in damage mechanics).

From the optimality of eq. (11) with respect to $\Delta\varepsilon^p$, we obtain that

$$Y_{\varepsilon^p} = -E(\nabla u_{n+1} - \varepsilon_n^p - \Delta\varepsilon^p) = -\sigma. \tag{12}$$

By making some rearrangement of the different terms in the integrals of eq. (11), optimality with respect to Δp and ΔP involves the Legendre-Fenchel transform of the norm $\sigma_0\|\cdot\|_q$, yielding the following plasticity yield criterion

$$\|(Y,Z)\|_q^* \leq \sigma_0, \quad \text{with} \quad Y = R + Y_p + \ell_0 \operatorname{div} Z, \quad R = -V'(p_n + \Delta p), \tag{13}$$

where $\|z\|_q^* = \sup_y\{y \cdot z,\ \|y\|_q \leq 1\}$ is the dual norm[2]. Combining constraints eqs. (12) and (13), we have

$$\begin{aligned} \|(Y,Z)\|_q^* &\leq \sigma_0 \\ |\sigma| &\leq Y - \ell_0 \operatorname{div} Z - R. \end{aligned} \tag{14}$$

Comparing with the plasticity yield criterion of the local model eq. (5), in the proposed regularized model, the initial yield stress σ_0 is replaced by $Y - \ell_0 \operatorname{div} Z$ where (Y, Z) belong to the ball $B = \{(y,z) \,|\, \|(y,z)\|_q^* \leq \sigma_0\}$ of radius σ_0. In addition, the same optimality with respect to Δp and ΔP from eq. (11) completes eq. (13) with the generalized flow rule and consistency condition

$$(\Delta p, \Delta P) \in N_B(Y,Z), \tag{15}$$

where N_B is the normal cone of B. Besides, by the last term of eq. (11), boundary conditions on $\partial\Omega = \{0, L\}$ are found to be

$$Z(0) = 0, \quad Z(L) = 0. \tag{16}$$

For clarity, the following set of equations in eq. (17) summarizes the first-order optimality conditions for the variational problem eq. (9):

equilibrium equation:	$\operatorname{div}\sigma = 0$	(Ω)	(17a)
plasticity yield criterion:	$(Y,Z) \in B$ $\lvert\sigma\rvert \leq Y - \ell_0 \operatorname{div} Z - R$	(Ω)	(17b)
flow rules and consistency conditions:	$(\Delta p, \Delta P) \in N_B(Y,Z)$ $\Delta\varepsilon^p(\lvert\sigma\rvert - Y + \ell_0 \operatorname{div} Z + R) = 0$ $\lvert\Delta\varepsilon^p\rvert = \Delta p, \quad \Delta P = \ell_0 \nabla \Delta p$	(Ω)	(17c)
Dirichlet boundary conditions:	$u(0) = 0, \quad u(L) = tL$	$(\partial\Omega)$	(17d)
Neumann boundary conditions:	$Z(0) = 0, \quad Z(L) = 0.$	$(\partial\Omega)$	(17e)

Note that the boundary conditions eq. (17e) are considered as Neumann conditions. This is consistent with not imposing any conditions on the plastic strain increment at either $x = 0$ or $x = L$.

Finally for completeness, non-smooth solutions may possibly exist and may exhibit jumps of Δp on several points $\Gamma = \{x_1, \dots x_J\} \subset \Omega$ (assuming by simplicity $\Gamma \not\subset \partial\Omega$). In this case, the incremental Lagrangian (11) should be extended with the extra term

[2]More precisely, we have $\|z\|_q^* = \|z\|_p$ where p is such that $\frac{1}{p} + \frac{1}{q} = 1$.

$$\sum_{j=1}^{J}\Big[\sigma_0\ell_0\,|[\![\Delta p(x_j)]\!]| + \ell_0 Z(x_j)[\![\Delta p(x_j)]\!]\Big], \tag{18}$$

where $[\![(\cdot)]\!]$ denotes a jump. When considering optimality, it results for every $x_j \in \Gamma$ in

$$\begin{aligned} &|Z(x_j)| \le \sigma_0 \\ &[\![\Delta p(x_j)]\!]\,(|Z(x_j)| - \sigma_0) = 0, \quad \text{with} \quad \operatorname{sgn}([\![\Delta p(x_j)]\!]) = \operatorname{sgn}(Z(x_j)), \end{aligned} \tag{19}$$

where $\operatorname{sgn}(\cdot)$ denotes the sign function.

Examples

If we select $q = 1$ (TV–norm) in the gradient-dependent dissipation potential, we end up with $\|\cdot\|_1^* = \|\cdot\|_\infty$ and the plasticity yield criterion is

$$\begin{aligned} &|Y| \le \sigma_0, \quad |Z| \le \sigma_0 \\ &|\sigma| \le Y - \ell_0 \operatorname{div} Z - R. \end{aligned} \tag{20}$$

If we select $q = \infty$, we have $\|\cdot\|_\infty^* = \|\cdot\|_1$ and

$$\begin{aligned} &|Y| + |Z| \le \sigma_0 \\ &|\sigma| \le Y - \ell_0 \operatorname{div} Z - R. \end{aligned} \tag{21}$$

3. Analytical solutions with the $\infty-$norm

We now aim at constructing a class of localized solutions to analyze the proposed model. We can exhibit explicit analytical solutions in the specific case of $q = \infty$ for the gradient-dependent dissipation potential eq. (8). Hence we consider, in the following,

$$\phi(\dot\varepsilon^p, \dot p, \dot P) = \sigma_0 \max\{\dot p, \ell_0|\nabla\dot p|\} + I_{\mathbb{R}^+}(\dot p - |\dot\varepsilon^p|). \tag{22}$$

As previously stated, we assume the tensile loading of a bar so that $p = \varepsilon^p$ and $\sigma > 0$, which remains constant due to the equilibrium condition with respect to displacement.

A symmetric localized plastic strain pattern is sought from the middle of the bar, so that $\dot p \ge 0$ and $\nabla\dot p \le 0$ if $L/2 \le x \le L$. We first address general properties of the sought localized solutions, independently of the exact form of the function $V(p)$, before being precised, at a later stage, as a bilinear function. For convenience, the equations are written in the time-continuous setting, and we introduce the change of variables $\hat x = (x - L/2)/\ell_0$, $\hat w = L/(2\ell_0)$, and consider the right-hand side of the bar $\hat x \in [0, \hat w]$.

3.1. General form of the solutions

By combining the yield criterion, the flow rules and the consistency conditions in eq. (17) for $q = \infty$, we have for all $\hat w \ge \hat x \ge 0$

$$\begin{aligned} Y - Z &= \sigma_0 \\ \sigma &= Y - \operatorname{div}_{\hat x} Z - R, \quad \text{with} \quad \operatorname{div}_{\hat x}(\cdot) = \ell_0 \operatorname{div}(\cdot) \\ \ell_0\nabla\dot p &= -\dot p. \end{aligned} \tag{23}$$

The last equality, between the plastic strain-rate and its gradient, can be integrated over $\hat{x}$ and t as

$$p = \overline{p} \exp\left(-\hat{x}\right), \tag{24}$$

where $\overline{p}$ represents the maximal plastic strain at the current time t, located in the middle of the bar at $\hat{x} = 0$. Moreover, the system of equations eq. (23) is completed by the boundary conditions eq. (16), which read here as

$$Z\left(0\right) = Z\left(\hat{w}\right) = 0, \tag{25}$$

the first, at $\hat{x} = 0$, coming from symmetric considerations. By using it, Z is found as:

$$Z = \left(\sigma - \sigma_0\right)\left(1 - \exp\left(\hat{x}\right)\right) - \int_0^{\hat{x}} R(p(y)) \exp\left(\hat{x} - y\right) \mathrm{d}y. \tag{26}$$

Moreover, by the boundary condition eq. (25) at $\hat{x} = \hat{w}$, the stress σ is found, with the help of a change of variable in the above integral, as:

$$\sigma = \sigma_0 + \frac{V(\overline{p}) - V\left(\overline{p} \exp\left(-\hat{w}\right)\right)}{\overline{p} - \overline{p} \exp\left(-\hat{w}\right)}. \tag{27}$$

In the limit $\hat{w} \ll 1$, the previous relationship is equivalent to $\sigma = \sigma_0 + V'(\overline{p}) = \sigma_0 - R(\overline{p})$, which recovers the homogeneous response if the regularization length scale ℓ_0 is large enough in comparison with the length of the bar L.

Considering the imposed displacement boundary conditions $u(0) = 0, u(L) = tL$, we have $\int_0^L \varepsilon(x)\mathrm{d}x = u(L) - u(0) = tL$, so that the displacement loading fixes the average amplitude of the plastic strain as

$$t = \int_{-\hat{w}}^{\hat{w}} \left(\frac{\sigma}{E} + \overline{p} \exp\left(-\left|\hat{x}\right|\right)\right) \mathrm{d}\hat{x} = \frac{\sigma}{E} + \frac{\overline{p}}{\hat{w}}\left(1 - \exp\left(-\hat{w}\right)\right), \tag{28}$$

where the symmetry of the plastic strain profile with respect to the middle of the bar has been imposed. Note that σ and $\overline{p}$ have been also previously related by eq. (27).

Now, we analyse the asymptotic state of the response at large plastic strains ($\overline{p} \gg \sigma_0/E$). At this stage, we assume that the negative isotropic hardening function behaves linearly, *i.e.* $V(p) \sim a - \sigma_0 p$ where a is a constant. In this situation, as observed from eq. (5), the current yield stress of the homogeneous response is $\sigma_p = \sigma_0 + V'(p) \to 0$. We can introduce thus E_u as being the total energy over the bar when the stress is approaching zero. It gathers both the dissipated energy[3] and the negative isotropic hardening energy, and can be computed as it follows:

[3]The monotonous loading allows to rewrite the dissipated energy from 0 to t, $\int_0^t \sigma_0 \max\{\dot{p}, \ell_0|\nabla\dot{p}|\}\mathrm{d}\tau$, as $\sigma_0 \max\{p, \ell_0|\nabla p|\}$ in eq. (29).

$$
\begin{aligned}
E_u &= \ell_0 \int_{-\hat{w}}^{\hat{w}} \left(V(p) + \sigma_0 \max\{p, \ell_0 |\nabla p|\}\right) \mathrm{d}\hat{x} \\
&= \ell_0 \int_{-\hat{w}}^{\hat{w}} \left(a - \sigma_0 \overline{p} \exp\left(-|\hat{x}|\right) + \sigma_0 \overline{p} \exp\left(-|\hat{x}|\right)\right) \mathrm{d}\hat{x} \\
&= (2\ell_0 \hat{w}) a = La.
\end{aligned}
\tag{29}
$$

Hence E_u does not depend on the length-like parameter ℓ_0, and keeps the same value as the energy from the homogeneous response (proportional to the bar L). This property will be illustrated here-after in Sections 3.2 and 4.2.

Let us summarize here some features of the exhibited analytical solutions. Firstly, the evolution of the plastic strain takes the form of decreasing exponential profiles eq. (24), the decay of which is controlled by ℓ_0. Therefore, the support of plastic strain is infinite. This stands in contrast to localized solutions more commonly found when using a quadratic term in the free energy as in eq. (1). More precisely, such formulations typically exhibit an initially finite support at localization, followed by a spreading phenomenon, especially in non-linear softening regimes (Jirásek and Rolshoven, 2009b; Scherer et al., 2019; Abatour and Forest, 2023). In the present dissipation-based regularization model with $q = \infty$, the localization process of cumulative plastic strains displays a stationary evolution: the ratio $p/\overline{p}$ eq. (24) remains indeed constant. Interestingly, the ultimate energy E_u eq. (29) is independent of ℓ_0, and recovers the one found by the homogeneous solution, proportional to the length L of the bar.

Remark. *We have assumed a smooth plastic strain profile without any jumps. With a closer investigation the jump condition eq.* (19)*, one can show that such non-smooth solutions cannot occur.*

3.2. The solutions for the bilinear softening

In order to analyze further the previous localized response, we now consider the bilinear negative isotropic hardening function,

$$
V(p) = V_{\mathrm{bi}}(p) = \begin{cases} -\dfrac{Hp^2}{2} & \text{if } p \leq \dfrac{\sigma_0}{H} \\ -\sigma_0 p + \dfrac{\sigma_0^2}{2H} & \text{otherwise,} \end{cases}
\tag{30}
$$

where $H > 0$ is the hardening modulus. By employing the function $V_{\mathrm{bi}}(p)$, one can easily show that the homogeneous softening response predicts a linear decrease of the stress from σ_0 to 0 with the prescribed displacement (Jirásek and Rolshoven, 2009b). In the case of localized solutions, the simplicity of $V_{\mathrm{bi}}(p)$ allows us to analyse more explicitly relationships eqs. (27) and (28). We can distinguish three different regimes, according to the value of the maximal plastic strain $\overline{p}$ in the middle of the bar.

- first regime (linear softening): the softening response begins, for which we have $\overline{p} \leq \sigma_0/H$, and thus $V_{\mathrm{bi}}(p) = -Hp^2/2$ at each position of the bar. We obtain easily by

eqs. (27) and (28) a linear relationship between the stress and the prescribed displacement,

$$\sigma = E\frac{t - \dfrac{2\sigma_0}{H\hat{w}}\tanh\left(\dfrac{\hat{w}}{2}\right)}{1 - \dfrac{2E}{H\hat{w}}\tanh\left(\dfrac{\hat{w}}{2}\right)}. \tag{31}$$

This regime ends as soon as $\overline{p} = \sigma_0/H$, which is equivalent, by eqs. (27) and (31), to the following values of the stress and of the displacement:

$$\begin{aligned} &\sigma = \sigma_{c1} = \frac{\sigma_0}{2}\left(1 - \exp\left(-\hat{w}\right)\right) \Longleftrightarrow \\ &t = t_{c1} = \frac{\sigma_0}{2E}\left(1 - \exp\left(-\hat{w}\right)\right)\left(1 - \frac{2E}{H\hat{w}}\tanh\left(\frac{\hat{w}}{2}\right)\right) + \frac{2\sigma_0}{H\hat{w}}\tanh\left(\frac{\hat{w}}{2}\right). \end{aligned} \tag{32}$$

- second regime (nonlinear softening): $\overline{p} \geq \sigma_0/H$, but we still assume $\overline{p}\exp(-\hat{w}) \leq \sigma_0/H$. Therefore, one must use $V_{\rm bi}(\overline{p}) = -\sigma_0\overline{p} + \sigma_0^2/(2H)$ which can allow us to express the stress after tedious calculations with eqs. (27) and (28). By letting A and B to be

$$\begin{aligned} A &= \exp(-\hat{w})\left(\frac{t\hat{w}H}{\exp\left(\hat{w}\right) - 1} - \sigma_0\right) \\ B &= \exp(-\hat{w})\left(\frac{\hat{w}H/E}{\exp\left(\hat{w}\right) - 1} - 1\right) + 1, \end{aligned} \tag{33}$$

the stress satisfies the following second-degree polynomial equation:

$$\left(\left(1 - \exp\left(-\hat{w}\right)\right)^2 - B^2\right)\sigma^2 + 2\left(\sigma_0\exp\left(-\hat{w}\right)\left(1 - \exp\left(-\hat{w}\right)\right) + AB\right)\sigma - A^2 = 0. \tag{34}$$

Thus, σ turns out to be a non-linear function of the displacement t. This regimes stops when $\overline{p}\exp(-\hat{w}) = \sigma_0/H$, which is equivalent, by eqs. (27) and (34), to

$$\sigma = \sigma_{c2} = 0 \Longleftrightarrow t = t_{c2} = \sigma_0\frac{\exp\left(\hat{w}\right) - 1}{\hat{w}H}. \tag{35}$$

- third regime (rupture): $\overline{p}\exp(-\hat{w}) \geq \sigma_0/H$: $V_{\rm bi}(p) = -\sigma_0\overline{p} + \sigma_0^2/(2H)$ at each position of the bar, so that for $t \geq t_{c2}$, one has $\sigma = \sigma_{c2} = 0$.

Figure 2a displays the elastic phase and the three previous softening phases of the stress-strain response for the local model parameters $E/\sigma_0 = 1000$ and $E/H = 5$, and a length ratio $\ell_0/L = 0.5$. Figure 2b compares the prediction for three different length ratios. One can note that the smaller ℓ_0/L, the larger the ultimate displacement t_{c2} for which there is rupture (the stress is zero), which is in agreement with (35). In parallel, a more prominent softening behaviour is predicted after the elastic regime, with an earlier non-linear evolution of the stress with the displacement. Figures 2c and 2d report similar comparisons for the

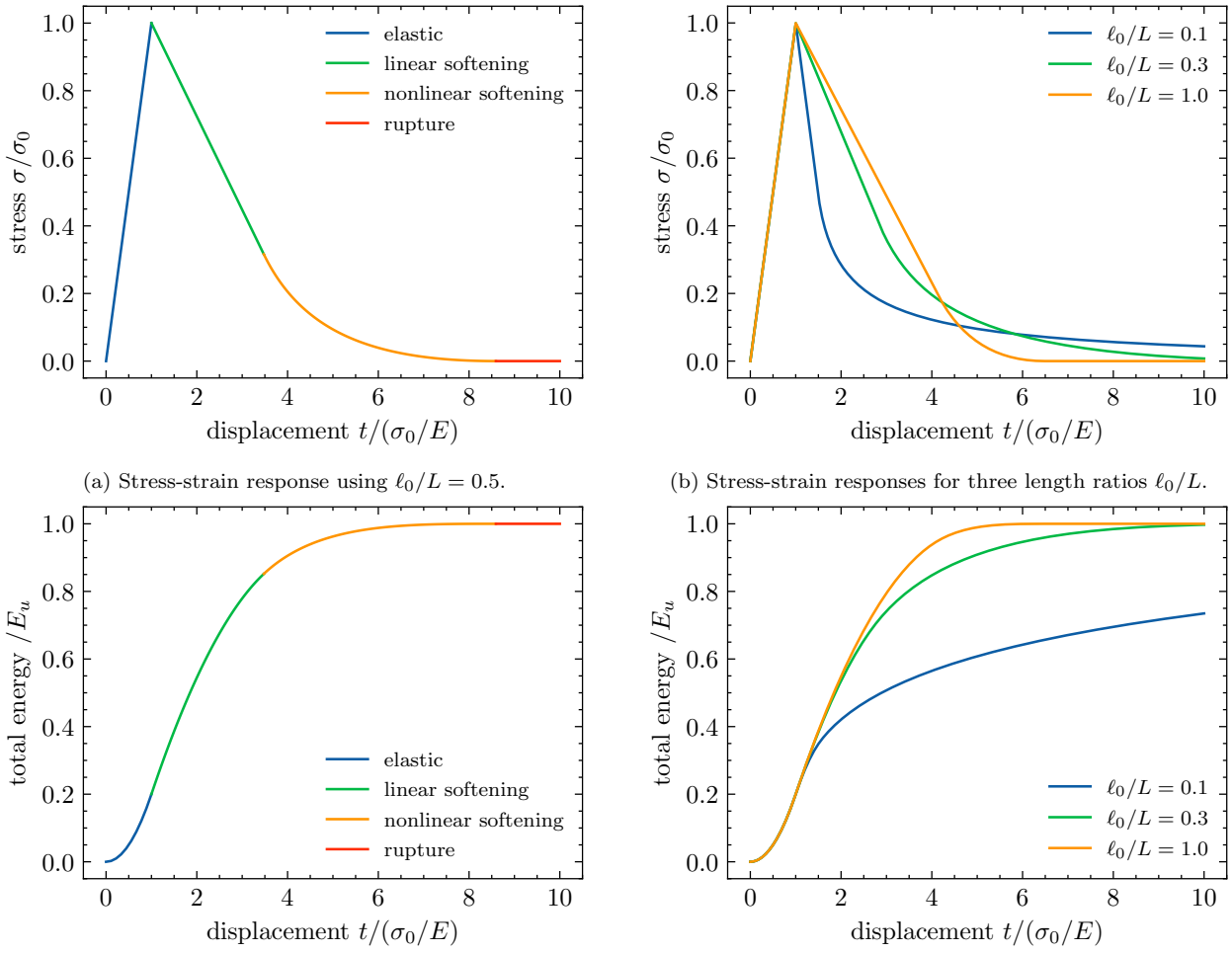

(a) Stress-strain response using $\ell_0/L = 0.5$.

(b) Stress-strain responses for three length ratios ℓ_0/L.

(c) Total energy evolution using $\ell_0/L = 0.5$.

(d) Total energy evolutions for three length ratios ℓ_0/L.

Figure 2: Analytical solutions.

evolution of the total energy. The energy tends toward its ultimate value $E_u = La$ with $a = \sigma_0^2/(2H)$ according to eqs. (29) and (30). However, for a fixed displacement t, the energy decreases with regards to the length ratio ℓ_0/L, even if E_u is independent of it.

In the analytical solutions illustrated in Figure 2, no snap-back is observed, due to the chosen values here for the model parameters. This specific feature will however be described later in Section 4.

4. One-dimensional numerical results

4.1. The numerical resolution

The previously derived solutions in Section 3.2 are now compared to numerical results. The numerical resolution of the incremental variational problem (9) is however not trivial. Indeed, due to the presence of the gradient term, the resolution of plastic strain evolution is not local anymore, as usual in strain-gradient plasticity models. In addition, the use of a q–norm dissipation potential instead of a quadratic gradient term brings yet another level of

complexity since the former is non-smooth, as opposed to the latter. A monolithic resolution using a standard global Newton-Raphson method is therefore doomed to fail due to the lack of differentiability.

Fortunately, conic optimization solvers have recently emerged as a viable alternative to solve difficult, highly non-smooth problems arising in various fields of mechanics, see for instance (Bleyer, 2022a) for an overview. In particular, classical elastoplastic evolution can be formulated in this framework, resulting in a convex second-order cone program. Dedicated primal-dual interior point solvers, such as Mosek for instance (MOSEK, 2019), can be leveraged for their resolution.

We use the same strategy in the present case. Here, the quadratic elastic energy and the gradient-dependent dissipation potential are both convex functions and can easily be expressed with the help of quadratic cones. However, when considering the negative isotropic hardening function, we are in presence of a concave function. More precisely, the softening incremental problem (9) can be formulated as minimizing the difference of two convex functions. This class of problem is called *difference of convex (DC) programming*. The most common and effective heuristic for finding local optima is the *convex-concave procedure*, see for example (Lipp and Boyd, 2016), which involves convexifying the concave function by linearizing it around a current iterate and solving the associated convex problem, then iterating. We use this strategy by linearizing $V(p)$ around a current estimate $p^{(k)}$ of the plastic strain, thereby replacing the non-convex function $V(p)$ with $V(p^{(k)}) + V'(p^{(k)})\Delta p$. In this procedure, the estimate $p^{(k)}$ is updated at each iteration of the convex-concave procedure. Convergence of the latter is obtained if the relative change of value of the objective function is less than 10^{-4}. In practice, we observe that the convex-concave procedure converges in less than 10 iterations on average. The flowchart in Algorithm 1 summarizes the procedure.

Similarly to (Bleyer, 2022a), we make use of the interior-point solver Mosek (MOSEK, 2019) and the FEniCS (Logg et al., 2012) software package for discretizing variational problems using the finite-element method combined into the `fenics_optim` package, see (Bleyer, 2020, 2022b). As spatial discretization is concerned, the displacement field u is discretized using a continuous quadratic Lagrange function space. The plastic strain field ε^p is discretized using a discontinuous piecewise affine space. Finally, due to the gradient term, the cumulative plastic strain p is discretized with a continuous linear Lagrange function space. A companion Zenodo repository (Bacquaert et al., 2024) accompanies the present paper to reproduce the one-dimensional tests from Sections 4.2 to 4.4.

Remark. *The cumulative plastic strain p and the plastic strain ε^p are interpolated separately. This separation is necessary to express the dissipation potential $\phi(\dot{\varepsilon}^p, \dot{p}, \dot{P})$ in eq.* (8) *by a proper constraint,* i.e. *the relaxed convex constraint $I_{\mathbb{R}^+}(\dot{p} - |\dot{\varepsilon}^p|)$. Consequently, only p must be regular enough to give a sense to $\dot{P} = \ell_0 \nabla \dot{p}$ (by a continuous linear interpolation), whereas a discontinuous interpolation can be used for ε^p.*

Algorithm 1 The iterative solution procedure.

Input: $(u_n, \varepsilon_n^p, p_n)$ at time t_n.
Output: $(u_{n+1}, \varepsilon_{n+1}^p = \varepsilon_n^p + \Delta\varepsilon^p, p_n + \Delta p)$ at time t_{n+1}.

Initialize iterations with $k = 0$ and $p^{(k)} = p_n$.

repeat
Linearize the negative hardening function: $V(p_n + \Delta p) \leftarrow V(p^{(k)}) + V'(p^{(k)})\Delta p$.
Solve the convexified minimization problem from *eq.* (9) for $(u_{n+1}, \Delta\varepsilon^p, \Delta p)$ with $p^{(k)}$.
Evaluate the value J_k of the objective function.
Update the estimate of the cumulative plastic strain: $p^{(k+1)} \leftarrow p_n + \Delta p$.
Set $k \leftarrow k + 1$.

until $|J_k - J_{k-1}| \leq \text{TOL}.|J_k|$. ▷ TOL. $= 10^{-4}$ is used in every numerical simulation.

4.2. Comparisons to the analytical solutions

First, we cross-validate the previous analytical solution and the numerical implementation on the case $q = \infty$ investigated in section 3 using the bilinear softening function $V_{\text{bi}}(p)$ eq. (30). The parameters of the constitutive model are first set to $E/\sigma_0 = 1000$, $E/H = 5$, and $\ell_0/L \in \{0.1, 0.3, 1\}$. In order to trigger a localized solution after the elastic regime, an imperfection on the initial yield stress σ_0 is introduced in the middle of the bar by decreasing it by 1 % in the region $[L/2 - d, L/2 + d]$ with $2d = L/100$. The prescribed displacement is discretized into 50 load-steps until $t = 10\sigma_0/E$ and the bar divided into 100 elements.

Figures 3a and 3b show the stress-strain responses and the total energy evolutions with the applied displacement. The analytical solutions and numerical results exhibit a perfect agreement.

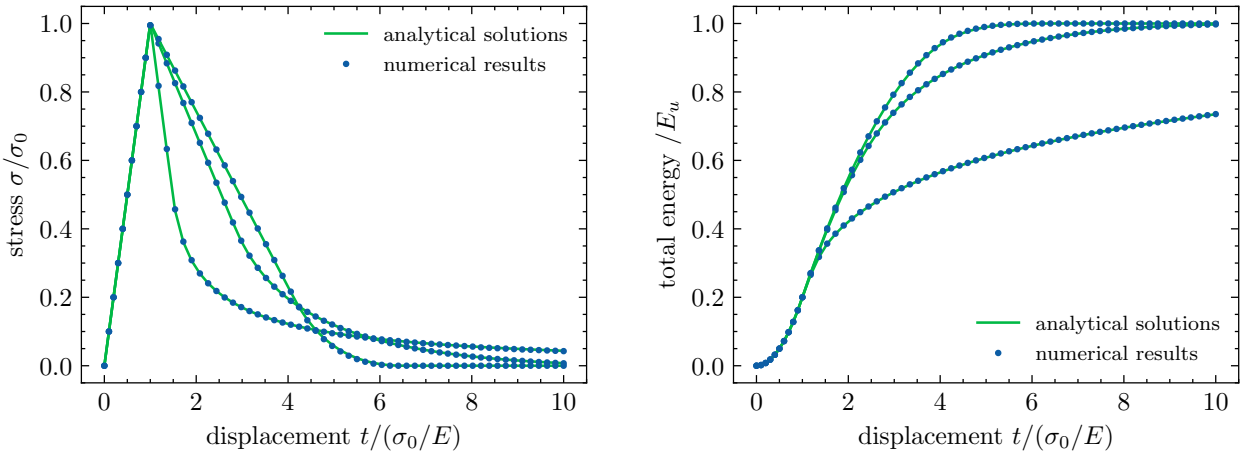

(a) Stress-strain responses.

(b) Total energy evolutions.

Figure 3: Comparisons of analytical solutions and numerical results for the stress response and the energy evolutions. Legend is reused from Figures 2b and 2d for each curve.

Figure 4 compares the plastic strain profiles for the three ratios ℓ_0/L. For $\ell_0/L = 0.1$ and

$\ell_0/L = 0.3$, analytical solutions in Figures 4a and 4b match the numerical results with the exponential profiles all along the loading. Again, the smaller ℓ_0, the more pronounced the decays of the plastic strain from the middle of the bar. In the case of $\ell_0/L = 1$, one can note apparently a mismatch between the numerical result and the analytical solution in Figure 4c. The numerical plastic profile is almost homogeneous late in the loading process. In fact, Figure 4d precises the instant at which this difference occurs. All along the loading phase for which $\sigma > 0$, the numerical result agrees with the analytical one (in green lines). After when $\sigma = 0$, the exponential profiles (in orange lines) no longer correspond to the numerical ones which, as seen in Figure 4c, increase homogeneously. Nevertheless, this difference of prediction does not impact the evolution of the total energy since, at this point the ultimate one E_u has been exactly reached as Figure 3b showed.

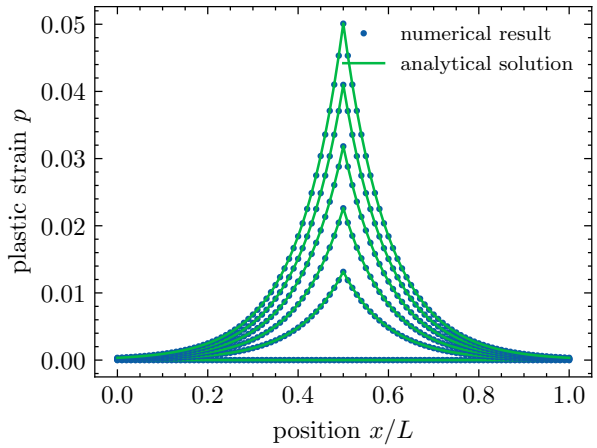

(a) Plastic strain profiles for $\ell_0/L = 0.1$.

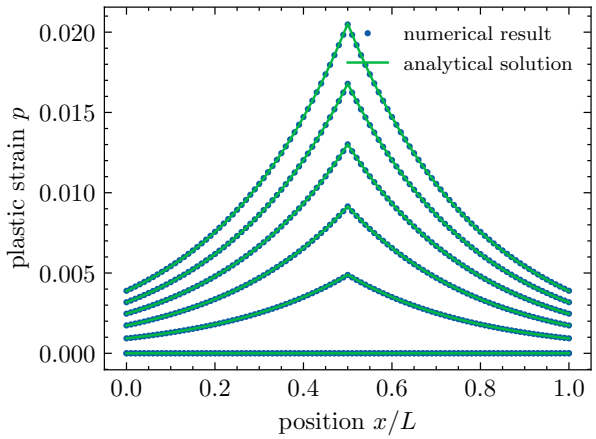

(b) Plastic strain profiles for $\ell_0/L = 0.3$.

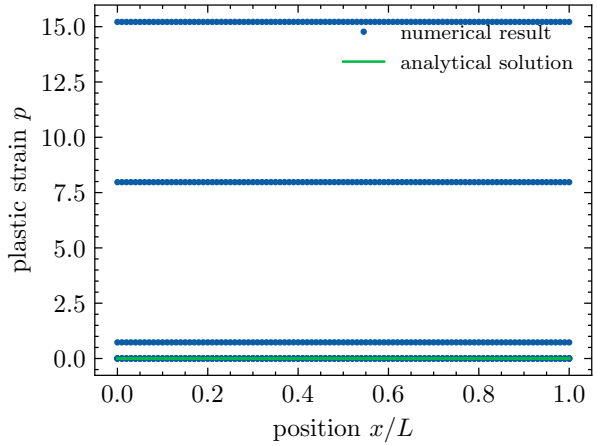

(c) Plastic strain profiles for $\ell_0/L = 1$.

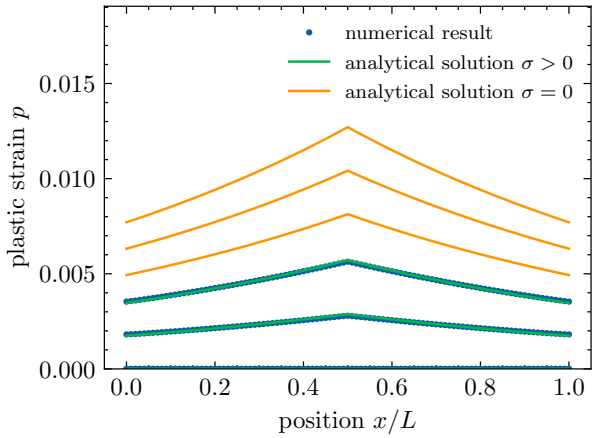

(d) Plastic strain profiles for $\ell_0/L = 1$ (zoom on the analytical solution near $\sigma = 0$).

Figure 4: Comparisons of analytical solutions and numerical results for the plastic strain profiles.

4.3. With snap-back responses

Here we select a higher hardening modulus H in order to observe softening responses with an initial snap-back after the elastic regime. To this goal, let us denote by $H_{\text{sb}} = 2E\tanh(\hat{w}/2)/\hat{w}$ ($\hat{w} = L/(2\ell_0)$) the minimal value of H for snap-back to occur, according to

eq. (31). The evolution of $H_{\rm sb}$ and the snap-back occurrence domain is displayed in Figure 5. Note that for an infinitely small bar ($\ell_0/L = \infty$), the condition of snap-back is the one of the homogeneous solution, *i.e.* $H/E > H_{\rm sb}/E = 1$.

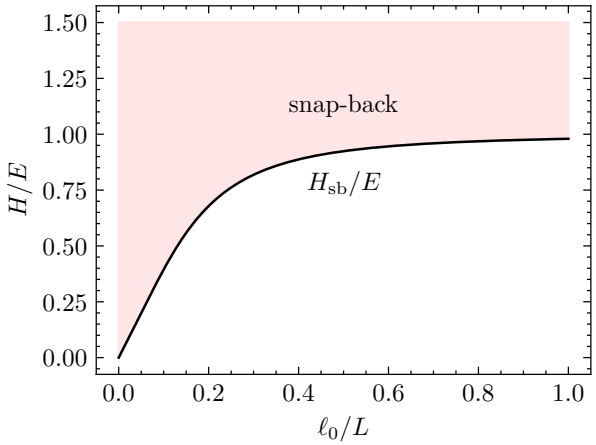

Figure 5: Phase-diagram showing the snap-back limit $H_{\rm sb}$ as a function of the ℓ_0/L and the relative hardening modulus H/E. Parameters in the upper pink zone lead to localized solution with snap-back.

We consider in the following $E/\sigma_0 = 1000, \ell_0/L = 0.2, H \in \{H_{\rm sb}/2, H_{\rm sb}, 2H_{\rm sb}, 4H_{\rm sb}\}$, and a displacement until $t = 3\sigma_0/E$ discretized by 50 load-steps. As above, a small imperfection is introduced in the middle of the bar, discretized by 100 elements.

Figures 6a and 6b compare the numerical results and the analytical solutions in terms of the stress and of the total energy. In the case of $H \geq H_{\rm sb}$, both numerical evolutions join the analytical predictions after the time-jump at the end of the elastic regime. This jump can also be illustrated in Figure 7, by plotting the plastic strain profiles for $H \in \{H_{\rm sb}, H_{\rm sb}\}$ near $t = \sigma_0/E$. One can note that the localization process starts from a strictly positive value of p in the middle of the bar.

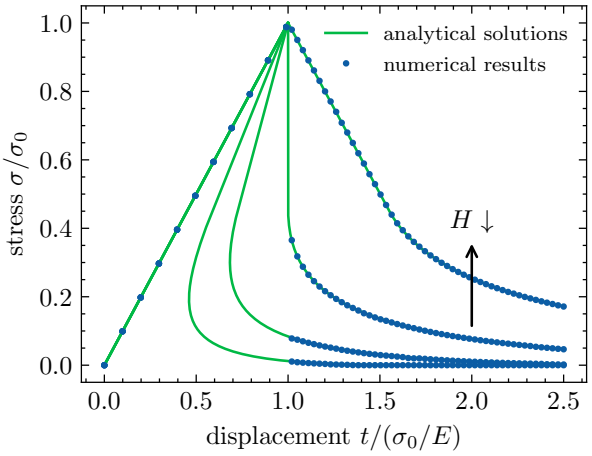

(a) Stress-strain responses.

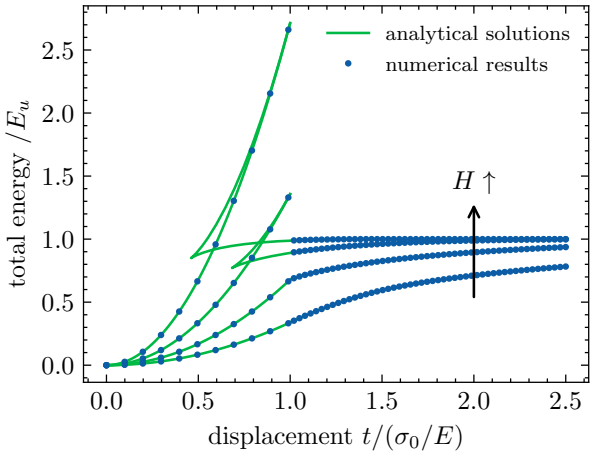

(b) Total energy evolutions.

Figure 6: Comparisons of analytical solutions and numerical results for the stress response and the energy evolutions by increasing the hardening modulus H such as $H \in \{H_{\rm sb}/2, H_{\rm sb}, 2H_{\rm sb}, 4H_{\rm sb}\}$.

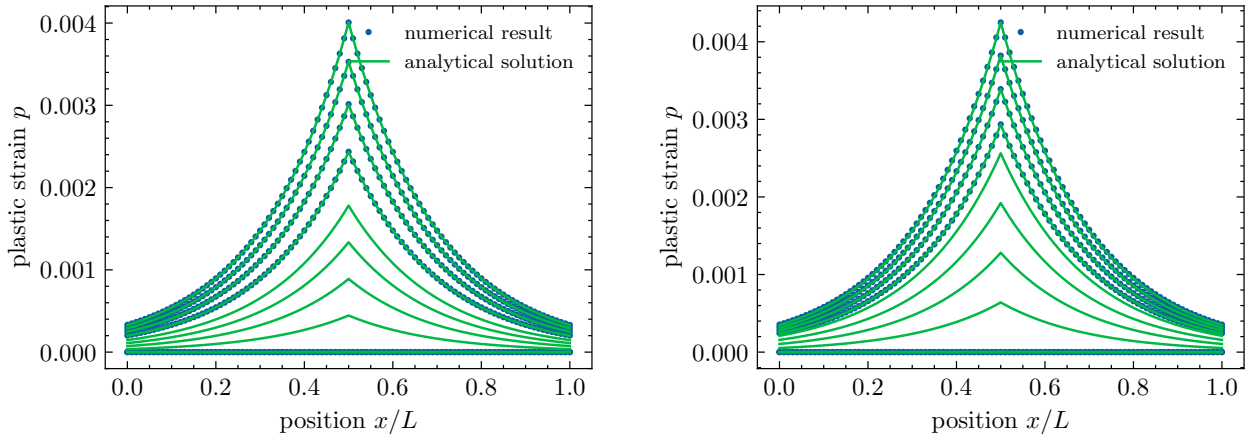

(a) Plastic strain profiles for $H/\sigma_0 = H_{\mathrm{sb}}/\sigma_0$ at $t/(\sigma_0/E) \leq 3/2$.

(b) Plastic strain profiles for $H/\sigma_0 = 2H_{\mathrm{sb}}/\sigma_0$ at $t/(\sigma_0/E) \leq 3/2$.

Figure 7: Comparisons of analytical solutions and numerical results for the plastic strain profiles in case of snap-back.

4.4. Numerical observations for the bilinear softening and some $q < \infty$–norms

Here, we briefly envision other q–norms as possible choices for the gradient-dependent dissipation potential. In the following, we use $q \in \{1.01, 1.2, 2, 4\} < \infty$ and the bilinear function $V_{\mathrm{bi}}(p)$. Note that conic programming solvers can perfectly accommodate all values of q between 1 and ∞ using power cones for instance, see again (Bleyer, 2022a). The parameters of the constitutive model are set to $E/\sigma_0 = 1000$, $E/H = 5$, and $\ell_0/L \in \{0.025, 0.05, 0.1\}$. The loading scenario stays the same as the one described in Section 4.2, with identical spatial and time discretization choices. However, in opposition to Section 4.2, Dirichlet boundary conditions are applied at both ends of the bar on the cumulative plastic strain ($p(0) = p(L) = 0$), which was found more effective for localization for several values of q compared to introducing a material imperfection.

Figure 8 shows the evolution of the plastic strain profiles over the loading time. For $q \geq 1.2$, the effect of ℓ_0 is clearly visible, increasing the width where the plastic strain is maximal. For $q = 1.2$, this maximum is reached in an area qualitatively resembling a plateau. For $q = 2$, the profile is more regular, without significant contrast, and resembles a harmonic function. For $q = 4$, the profile is more angular in the middle of the bar, similar to the exponential profile obtained for $q = \infty$ (see Figure 4). However, for $q = 1.01$, the effect of ℓ_0 is almost negligible, especially for $\ell_0/L = 0.05$ and $\ell_0/L = 0.1$. The plastic strain occupies almost the entire bar, except for the extremities where Dirichlet boundary conditions are applied.

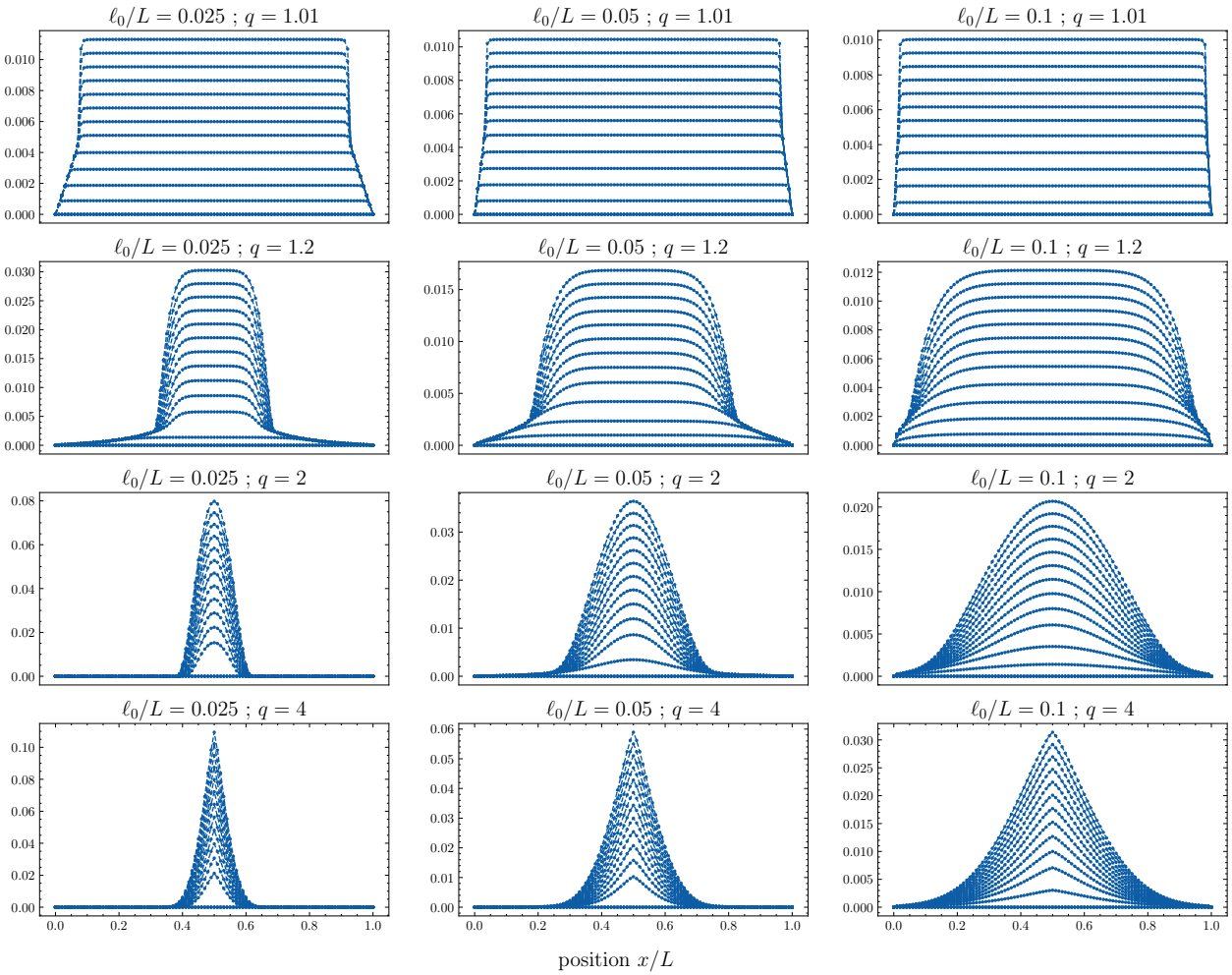

Figure 8: Plastic strain profiles for different $q < \infty-$norms and lengths ratios ℓ_0/L.

Figure 9 displays the force responses for $q \in \{1.01, 2, 4\}$. For $q = 2$ and $q = 4$, the higher the value of ℓ_0, the less brittle the softening response becomes. For $q = 1.01$, this is less evident, as the softening regimes appear linear with the same slope. Additionally, the maximum yield stress at the end of the elastic regime exceeds σ_0, with an increasing excess for larger ℓ_0. This is the well-known strengthening-size effect from plastic flow constraints (here $p(0) = p(L) = 0$), which can be found in numerous strain gradient plasticity models due to the use linear-growth nonlocal energies (Anand et al., 2005; Chiricotto et al., 2016; Dahlberg and Ortiz, 2019; Reddy and Sysala, 2023).

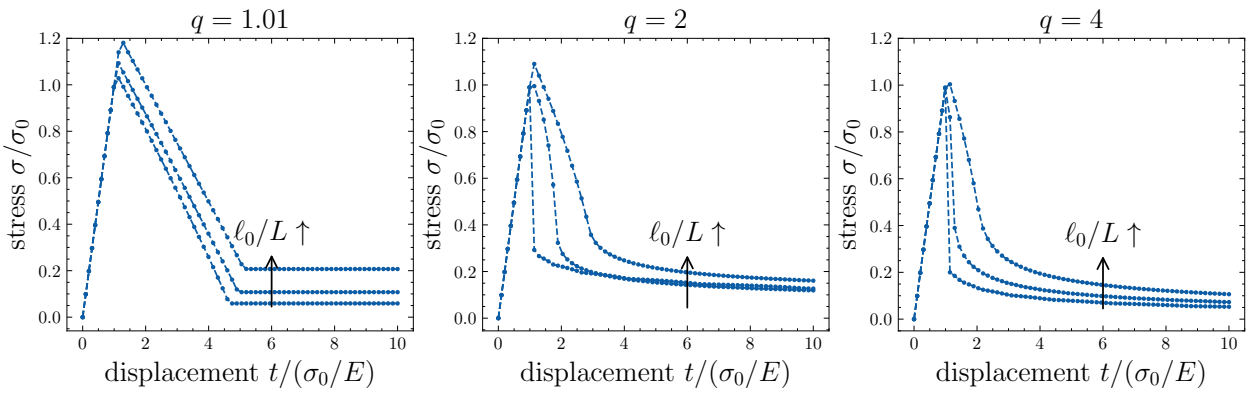

Figure 9: Stress-strain responses for different q–norms. The length ratios ℓ_0/L from Figure 8 are reused for each value of q.

5. A two-dimensional example

5.1. Constitutive equations for von Mises plasticity

The one-dimensional plasticity model is now straightforwardly extended to von Mises plasticity. To this goal, the following free energy and gradient-dependent dissipation potentials are considered:

$$\begin{cases} \psi(\boldsymbol{\varepsilon}, \boldsymbol{\varepsilon}^p, p) = \dfrac{\kappa}{2} \operatorname{tr}(\boldsymbol{\varepsilon} - \boldsymbol{\varepsilon}^p)^2 + \mu \operatorname{dev}(\boldsymbol{\varepsilon} - \boldsymbol{\varepsilon}^p) : \operatorname{dev}(\boldsymbol{\varepsilon} - \boldsymbol{\varepsilon}^p) + V(p) & \text{(36a)} \\ \phi(\dot{\boldsymbol{\varepsilon}}^p, \dot{p}, \dot{P}) = \sigma_0 \|(\dot{p}, \dot{P})\|_q + I_{\mathbb{R}^+}(\dot{p} - \|\dot{\boldsymbol{\varepsilon}}^p\|) + I_{\{0\}}(\operatorname{tr} \dot{\boldsymbol{\varepsilon}}^p), & \text{(36b)} \end{cases}$$

with $\dot{P} = \ell_0 \nabla \dot{p}$ and $I_{\{0\}}$ the characteristic function of $\{0\}$. μ and κ are the shear and the bulk moduli. $\operatorname{dev} \boldsymbol{x}$ is the deviatoric part of $\boldsymbol{x}$, $\operatorname{tr} \boldsymbol{x}$ its trace. In the present example, as in Section 3, the gradient-dependent dissipation potential is chosen to be $q = \infty$ and we use the bilinear hardening function (30) for $V(p)$.

5.2. Plane strain tension test

The loading scenario under consideration closely aligns with the one detailed by Anand (2012): a specimen with a rectangular cross-section, characterized by edge-lengths $a = 20\,\text{mm}$ and $3a/2 = 30\,\text{mm}$, undergoes stretching in plane strain conditions. The bottom edge is clamped, while the top edge is subjected to a prescribed condition of no horizontal displacement and an increasing vertical component $\overline{U}$. Left and right edges are traction-free. The material parameters are summarized in Table 1.

κ (GPa)	μ (GPa)	σ_0 (MPa)	H (GPa)	ℓ_0 (mm)
150	70	200	20/50/200	2

Table 1: Material parameters of the von Mises constitutive model.

As for the bar in traction in 1D, the finite element discretization employs quadratic elements for the displacement vector $\boldsymbol{u}$. The cumulative plastic strain p is discretized using

linear elements, while a discontinuous piecewise interpolation is employed for the plastic strain tensor $\boldsymbol{\varepsilon}^p$.

To investigate the mesh sensitivity of the model, we employ four unstructured triangular meshes by varying the element size h_{mesh}, such as $\ell_0/h_{\text{mesh}} \in \{1, 2, 4, 8\}$. In Figure 10a, the force-versus-displacement curves resulting from simulations on the different meshes are presented, while Figure 10b illustrates the evolution of the total energy. In the Figures, two hardening moduli $H \in \{20, 200\,\text{MPa}\}$ are considered. These findings demonstrate a very good convergence with respect to mesh refinement. Notably, the force and total energy exhibit minimal sensitivity to the largest mesh size employed. For the higher modulus $H = 200\,\text{MPa}$ one observes a time-jump after the elastic regime until about $\overline{U} = 0.03\,\text{mm}$. At this instant, the total energy immediately decreases during this time-step. This evolution is completely reminiscent of the snap-back ones for the bar in traction in 1D. For the lower modulus $H = 20\,\text{MPa}$, no snap-back is visible, and the total energy increases monotonously. Additionally, on the finest mesh ($\ell_0/h_{\text{mesh}} = 8$), Figure 11 illustrates the isovalues of the cumulative plastic strain for three different instants. Interestingly, the patterns change according to the value of H. One can observe localization patterns with either inclined or horizontal crossing bands, with maximal values of p either in the bulk of the plate or at its left and right edges.

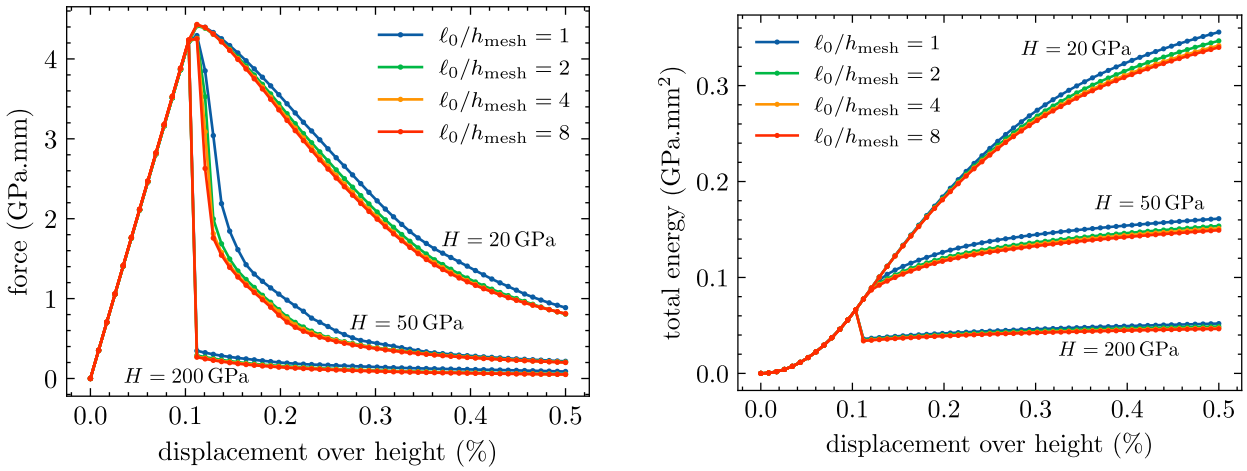

(a) Force response.

(b) Dissipated energy.

Figure 10: Effect of the mesh size refinement in the simulations.

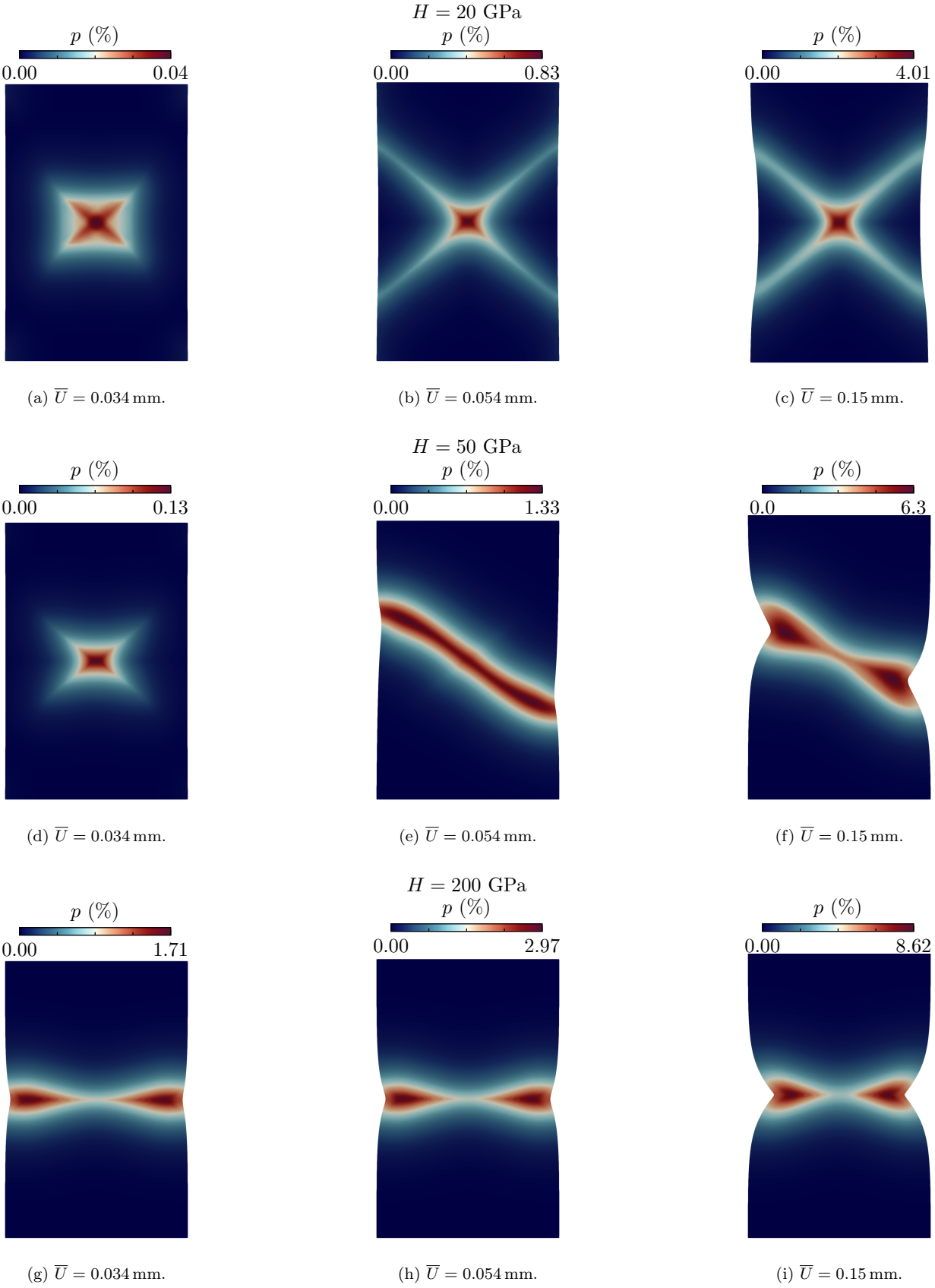

(a) $\overline{U} = 0.034\,\text{mm}$. (b) $\overline{U} = 0.054\,\text{mm}$. (c) $\overline{U} = 0.15\,\text{mm}$.

(d) $\overline{U} = 0.034\,\text{mm}$. (e) $\overline{U} = 0.054\,\text{mm}$. (f) $\overline{U} = 0.15\,\text{mm}$.

(g) $\overline{U} = 0.034\,\text{mm}$. (h) $\overline{U} = 0.054\,\text{mm}$. (i) $\overline{U} = 0.15\,\text{mm}$.

Figure 11: Isovalues of the cumulative plastic strain on the most finest mesh ($\ell_0/h_{\text{mesh}} = 8$) at three instants on the deformed configuration of the plate magnified by a factor 10.

6. Conclusion

In this work, we proposed a regularization approach for softening plasticity within the framework of Generalized Standard Materials. To achieve this, we introduced a cumulative plastic strain-rate gradient into the dissipation potential. We formulated an incremental variational formulation focusing on a one-dimensional problem. For the special norm $q = \infty$, we considered the traction of a homogeneous bar to derive analytical solutions with localization. Specifically, we found exponential profiles whatever the specific expression of the negative isotropic hardening function. This represents a pivotal aspect of the regularization approach, as other models featuring a quadratic gradient term in the free energy do not exhibit the same characteristic in case of non-linear strain-softening. In addition, it was shown that the regularization approach was able to predict a well-controlled evolution of the total energy, which interestingly turns out to be independent of the introduced length-like parameter at break. Numerical tests were conducted under the scope of conic programmings to validate the analytical solutions exhibited in the case of a bilinear softening law. By a simple generalization to the multi-dimensional case, the regularization approach was applied on von Mises plasticity. The stretch of a rectangular specimen was performed under plane strain conditions. Excellent results were found with mesh refinement, underscoring the relevance and efficiency of the regularization approach. Future works will consider applications on more sophisticated constitutive behaviours, for example taking into account the mean stress dependency in yield criteria as it is relevant for geomaterials, as well as more numerical experiments. Other norms $q < \infty$ will also be the subject of further studies as the ones sketched in Section 4.4.

References

Abatour, M., Forest, S., 2023. Strain gradient plasticity based on saturating variables. European Journal of Mechanics - A/Solids , 105016.

Aifantis, E.C., 1987. The physics of plastic deformation. International Journal of Plasticity 3, 211–247.

Alessi, R., Marigo, J.J., Maurini, C., Vidoli, S., 2018. Coupling damage and plasticity for a phase-field regularisation of brittle, cohesive and ductile fracture: One-dimensional examples. International Journal of Mechanical Sciences 149, 559–576.

Alessi, R., Marigo, J.J., Vidoli, S., 2015. Gradient damage models coupled with plasticity: Variational formulation and main properties. Mechanics of Materials 80, 351–367. Materials and Interfaces.

Anand, L., 2012. A large-deformation gradient theory for elastic–plastic materials: Strain softening and regularization of shear bands. International Journal of Plasticity 30-31, 116–143.

Anand, L., Gurtin, M.E., Lele, S.P., Gething, C., 2005. A one-dimensional theory of strain-gradient plasticity: Formulation, analysis, numerical results. Journal of the Mechanics and Physics of Solids 53, 1789–1826.

Andrieux, S., Joussemet, M., Lorentz, E., 1996. A class of constitutive relations with internal variable derivatives : derivation from homogenization. Comptes rendus de l'Académie des sciences 323, 629–636.

Bacquaert, G., Bleyer, J., Maurini, C., 2024. Regularization of softening plasticity with the cumulative plastic strain-rate gradient: companion software. URL: `https://doi.org/10.5281/zenodo.13893469`, doi:10.5281/zenodo.13893469.

Besson, J., Bleyer, J., Feld-Payet, S., Gourgues-Lorenzon, A.F., Hannard, F., Helfer, T., Hure, J., Kondo, D., Lazarus, V., Le Bourlot, C., Maitournam, H., Maurini, C., Moes, N., Morgeneyer, T., Morin, L., Petit, T., Simar, A., 2023. MEALOR II Damage Mechanics and Local Approach to Fracture. Zenodo. URL: `https://doi.org/10.5281/zenodo.10125170`.

Bleyer, J., 2020. Automating the Formulation and Resolution of Convex Variational Problems: Applications from Image Processing to Computational Mechanics. ACM Transactions on Mathematical Software (TOMS) 46, 1–33.

Bleyer, J., 2022a. Applications of Conic Programming in Non-smooth Mechanics. Journal of Optimization Theory and Applications .

Bleyer, J., 2022b. fenics_optim – Convex optimization interface in FEniCS. URL: `https://doi.org/10.5281/zenodo.5833932`, doi:10.5281/zenodo.5833932.

de Borst, R., Sluys, L., Mühlhaus, H.B., Pamin, J., 1993. Fundamental issues in finite element analyses of localization of deformation. Engineering Computations 10, 99–121.

Bourdin, B., Francfort, G., Marigo, J.J., 2000. Numerical experiments in revisited brittle fracture. Journal of the Mechanics and Physics of Solids 48, 797–826.

Bourdin, B., Francfort, G., Marigo, J.J., 2008. The Variational Approach to Fracture. Journal of Elasticity 91, 5–148.

Chambon, R., Caillerie, D., El Hassan, N., 1998. One-dimensional localisation studied with a second grade model. European Journal of Mechanics - A/Solids 17, 637–656.

Chiricotto, M., Giacomelli, L., Tomassetti, G., 2016. Dissipative scale effects in strain-gradient plasticity: The case of simple shear. SIAM Journal on Applied Mathematics 76, 688–704.

Dahlberg, C., Ortiz, M., 2019. Fractional strain-gradient plasticity. European Journal of Mechanics - A/Solids 75, 348–354.

Engelen, R., Geers, M., Baaijens, F., 2003. Nonlocal implicit gradient-enhanced elasto-plasticity for the modelling of softening behaviour. International Journal of Plasticity 19, 403–433.

Fernandes, R., 2008. A simplified second gradient model for dilatant materials: Theory and numerical implementation. International Journal of Solids and Structures 45, 5289–5307.

Fleck, N.A., Muller, G.M., Ashby, M.F., Hutchinson, J.W., 1994. Strain gradient plasticity: Theory and experiment. Acta Metallurgica et Materialia 42, 475–487.

Forest, S., 2009. Micromorphic Approach for Gradient Elasticity, Viscoplasticity, and Damage. Journal of Engineering Mechanics 135, 117–131.

Frémond, M., Nedjar, B., 1996. Damage, gradient of damage and principle of virtual power. International Journal of Solids and Structures 33, 1083–1103.

Gurtin, M.E., Anand, L., 2009. Thermodynamics applied to gradient theories involving the accumulated plastic strain: The theories of Aifantis and Fleck and Hutchinson and their generalization. Journal of the Mechanics and Physics of Solids 57, 405–421.

Halphen, B., Nguyen, Q.S., 1975. Sur les matériaux standard généralisés. Journal de Mécanique 14, 39–63.

Jirásek, M., Rolshoven, S., 2009a. Localization properties of strain-softening gradient plasticity models. Part I: Strain-gradient theories. International Journal of Solids and Structures 46, 2225–2238.

Jirásek, M., Rolshoven, S., 2009b. Localization properties of strain-softening gradient plasticity models. Part II: Theories with gradients of internal variables. International Journal of Solids and Structures 46, 2239–2254.

Lipp, T., Boyd, S., 2016. Variations and extension of the convex–concave procedure. Optimization and Engineering 17, 263–287.

Logg, A., Mardal, K.A., Wells, G., 2012. Automated Solution of Differential Equations by the Finite Element Method: The FEniCS Book. 1 ed., Springer Berlin, Heidelberg.

Lorentz, E., Andrieux, S., 1999. A variational formulation for nonlocal damage models. International Journal of Plasticity 15, 119–138.

Maugin, G.A., 1990. Internal Variables and Dissipative Structures. Journal of Non-Equilibrium Thermodynamics 15, 173–192.

Mialon, P., 1986. Éléments d'analyse et de résolution numérique des relations de l'élastoplasticité. bulletin de la DER, série C mathématiques informatique 3, 57–89. EDF.

Miehe, C., Aldakheel, F., Raina, A., 2016. Phase field modeling of ductile fracture at finite strains: A variational gradient-extended plasticity-damage theory. International Journal of Plasticity 84, 1–32.

MOSEK, 2019. The MOSEK Optimizer API for Python.Version 9.3. URL: `https://docs.mosek.com/9.3/pythonapi/index.html`.

Mühlhaus, H., Vardoulakis, I., 1987. The thickness of shear bands in granular materials. Géotechnique 37, 271–283.

Needleman, A., Tvergaard, V., 1998. Dynamic crack growth in a nonlocal progressively cavitating solid. European Journal of Mechanics - A/Solids 17, 421–438.

Nguyen, Q.S., 2011. Variational Principles in the Theory of Gradient Plasticity. Comptes Rendus Mécanique 339, 743–750.

Nguyen, Q.S., 2021. On standard gradient plasticity and visco-plasticity. International Journal of Solids and Structures 225, 111038.

Ortiz, M., Stainier, L., 1999. The variational formulation of viscoplastic constitutive updates. Computer Methods in Applied Mechanics and Engineering 171, 419–444.

Pham, K., Amor, H., Marigo, J.J., Maurini, C., 2011. Gradient damage models and their use to approximate brittle fracture. International Journal of Damage Mechanics 20, 618–652.

Pijaudier-Cabot, G., Bažant, Z.P., 1987. Nonlocal Damage Theory. Journal of Engineering Mechanics 113, 1512–1533.

Reddy, B.D., Sysala, S., 2023. The elastic threshold for strain-gradient plasticity, and comparison of theoretical results with experiments. European Journal of Mechanics - A/Solids , 105025.

Russo, R., Girot M., F.A., Forest, S., Jacquin, D., 2020. A Review on Strain Gradient Plasticity Approaches in Simulation of Manufacturing Processes. Journal of Manufacturing and Materials Processing 4.

Scherer, J.M., Besson, J., Forest, S., Hure, J., Tanguy, B., 2019. Strain gradient crystal plasticity with evolving length scale: Application to voided irradiated materials. European Journal of Mechanics - A/Solids 77, 103768.

Suquet, P., 1981. Sur les équations de la plasticité : existence et régularité des solutions. Journal de Mécanique 20, 3–39.